Fuel 310 (2022) 122246

Contents lists available at ScienceDirect

Fuel

journal homepage: www.elsevier.com/locate/fuel

Full length article

Numerical investigation of glycerol/diesel emulsion combustion in compression ignition conditions using Stochastic Reactor Model

Michał T. Lewandowski *, Corinna Netzer, David R. Emberson, Terese Løvås

Department of Energy and Process Engineering, NTNU Norwegian University of Science and Technology, Trondheim, Norway

ARTICLE INFO

Keywords:
Stochastic Reactor Model
Glycerol
Soot
ICE
Modelling
Particulate mater

ABSTRACT

In this work, we numerically investigate the potential of glycerol as a diesel fuel additive to reduce soot emissions. Many different fuel additives offer environmental benefits, since there is a surplus supply of glycerol as a by-product of biodiesel production, it is considered as a promising available candidate. The combustion process of glycerol in a direct injection compression ignition engine has been previously investigated experimentally for a 10 % (vol) glycerol emulsion. Based on the experimental set-up, a zero-dimensional Stochastic Reactor Model (SRM) is constructed to conduct numerical analysis with a detailed chemical mechanism for the combustion of hydrocarbon and oxygenated fuels. Applied models are presented and discussed with a focus on the characteristic mixing time scale of micromixing closure which is calculated using a 0D k-ϵ. The model constants are optimized to the analysed engine with the aid of a genetic algorithm and the sensitivity analysis is presented. For both fuels, emissions of major species are reproduced well but NO_x results are slightly overestimated. Emissions of carbon monoxide are predicted well for the reference diesel fuel, but the SRM does not capture the trend of increased CO with glycerol emulsion. The stochastic nature of the model is used to represent the mixture inhomogeneity, and the results are analysed using equivalence ratio–temperature plots to identify soot promoting conditions. The evolution of selected soot precursor and oxidizers is analysed, showing the capability of glycerol to reduce the former and increase the latter with a moderate effect. Soot formation and decomposition rates are presented, with very similar behaviour for both fuels. A shorter combustion phasing for the glycerol emulsion was observed and identified as the main contributory factor that led to the soot reduction while the chemical effect i.e oxygen content of the glycerol was present but not the dominant factor. The soot model results do not provide any evidence for the origin of experimentally observed small-sized particles, but it is discussed that the emissions results indicate the presence of low volatile compounds that could condense in the exhaust system.

1. Introduction

In diesel engines, particulate matter (PM) and nitrogen oxides (NO_x) emissions are a big concern. The non-premixed combustion nature in Direct Injection Compression Ignition (DICI) engines imposes the problem of searching for a compromise between PM and NO_x production. This compromise can be achieved by implementing new combustion modes using Low-Temperature strategies [1] such as Homogeneous Charge Compression Ignition (HCCI), Reactivity Controlled Compression Ignition (RCCI), partially-premixed compression ignition (PPCI), or Gasoline Compression Ignition (GCI). Emissions reductions can also be achieved by introducing new sustainable fuels, or fuel additives [2]. Fuel additives can be added to promote combustion processes, such as octane number improvers (used in SI engines to run at high compression ratios); oxygenated additives, used to assist in PM suppression or as corrosion inhibitors [3].

Wider utilization of bio-based energy carriers results in large number of different liquid biofuels and their by-products. Biodiesel fuels are reported to have a positive trend in emission reduction but with some concern about increased number of small particles [4]. In general, so-called oxygenated fuels i.e. whose molecule contains oxygen atoms, poses advantageous properties. Fuel additives which increase fuel-born oxygen have been investigated as well. For example, Rounce et al. [5] have shown that dimethyl carbonate (DMC) reduced THCs, CO, and PM by up to 50% with a blend of 96% diesel and just 4% DMC by mass. Kozak et al. [6] studied the influence of oxygenated diesel fuels on PM/NO_x emission trade-off. They pointed out that the reduction in PM emissions does not depend only on the oxygen content in fuel but also on the oxygenate type and its properties. They concluded that diethyl maleate, dimethyl carbonate, and diethyl carbonate had been

* Corresponding author.
E-mail address: michalew@ntnu.no (M.T. Lewandowski).

https://doi.org/10.1016/j.fuel.2021.122246
Received 10 July 2021; Received in revised form 24 September 2021; Accepted 7 October 2021

the most promising oxygenate compounds as blending components in diesel fuel. Recently, Sidhu et al. [7] presented an experimental study on performance and emissions of diesel–biodiesel blends and their emulsions with glycerine.

The increased production of biodiesel over the previous years led to a surplus of the glycerol by-product [8]. This glycerol is refereed to as crude glycerol and will contain many impurities associated with the transesterification process [9]. Glycerol is the pure chemical compound 1,2,3 propanetriol, while "glycerin" usually applies to a purified commercial product with contents of higher than 95% glycerol. Many grades of glycerin are commercially available; obtained after removal of salts, methanol, and free fatty acids. In most commercial applications the quality of glycerin must be improved until it has an acceptable purity that is completely different from those obtained in biodiesel facilities [10].

Recently Nda-Umar et al. [11] reviewed options of potential usage of glycerol to improve the overall economics of biodiesel production. Conversion of glycerol to high-value products in biofuels, fuel additives and other bio-based chemicals was considered. The use of glycerol as a fuel or as a fuel additive is one of the viable and attractive options. The challenge to utilize glycerol as a fuel additive is that it is comparatively difficult to burn due in part to its low energy density, its high viscosity, and high auto-ignition temperature. Relevant research on the combustion performance of glycerol is required to facilitate its future utilization as a fuel additive.

Eaton et al. [12] experimentally investigated a glycerol–diesel emulsion and characterized the resulting fuel properties. Emulsions with 10 and 20% content of glycerol were burnt in a naturally aspirated single-cylinder diesel engine showing a reduction of NO_x and PMs by 5–15 and 25%–50%, respectively. The work reported an increase in fuel consumption, due to the reduced LHV of the emulsions compared to pure diesel and an increase in the thermal efficiency at high loads. Using constant volume reactor simulations, Jach et al. [13] studied the effect of glycerol doping on the ignition delay times (IDT) and laminar burning velocities of both diesel and gasoline fuels. They shown that significant changes in IDT of n-heptane/glycerol mixture (representing diesel fuel) can be observed when the molar fraction of glycerol is higher than 50% and concluded that glycerol addition at lower molar fractions should not have a detrimental effect on ignition. Recently, Eaton et al. [14] investigated utilization and performance of glycerol–biodiesel emulsion (23 wt% glycerol) in a one-megawatt, six-cylinder marine engine. They have demonstrated that glycerol-based emulsion fuel can be compatible with existing large-bore diesel engines and can reduce the carbon footprint of marine propulsion systems and stationary power generators. They have also pointed out that glycerol significantly reduced observable smoke but led to an increase in soot particles smaller than 2.5 μm. Recently, Emberson et al. [15] examined combustion of diesel and glycerol emulsions under compression ignition conditions to demonstrate potential to suppress the soot formation. Their experiments were performed in an automotive engine and in an optical combustion chamber. They have presented soot emissions measuring exhaust particle size distributions but also in-flame soot characteristics. Instead of utilizing crude glycerol, Szori et al. [16] proposed to use glycerol carbonate as a more suitable fuel additive. They have performed theoretical consideration showing that glycerol carbonate decomposes mainly to carbondioxide and 3-hydroxypropanal. Consequently, the higher concentration of aldehydes potentially can have a considerable effect on soot reduction. On the other hand, we expect problems in practical utilization of that fuel additive due to difficulties in obtaining stable emulsion with standard diesel fuel.

Various simulation methodologies can be applied to investigate the influence of fuel additives on combustion performance and emissions considering, both physical and chemical properties of the fuel. Methods emulating realistic in-cylinder conditions where fuel performance can be tested using detailed chemical kinetic schemes are especially attractive. Commonly used constant pressure or constant volume reactor approaches to mimic engine conditions have certain limitations. A more sophisticated approach is to represent the in-cylinder gas as an ensemble of notional particles within the Stochastic Reactor Model (SRM) approach, which has been intensively developed in recent years [17–22]. There are numerous studies using SRM to investigate novel fuels, Matrisciano et al. [23] conducted an experimentally and numerically investigation applying an SRM for diesel and biodiesel fuel blends in a single-cylinder DI Diesel engine at one engine operating point. The work showed that the DI-SRM is capable of simulating the Diesel engine combustion process and accurately predicting exhaust emissions. Yasar et al. [24] have used SRM in conjunction with experimental data to investigate the performance of the HCCI engine. They achieved very good in-cylinder pressure results compared to the experiment and relatively well reproduced emission trends for several equivalence ratios. Ahmedi et al. [25], using SRM, investigated premixed compression ignition combustion mode. They employed a three component surrogate model to simulate five different fuels, where the blending proportions were based on the auto-ignition characteristics of the fuel used in the experimental work. They reported that the model gave satisfactory results in terms of in-cylinder pressure, heat release rate, combustion phasing parameters, and pollutant emissions and provided a better understanding of the PCI combustion process. Maurya and Mishra [26] successfully used the SRM approach in their parametric study of dual fuel (natural gas port injection and diesel pilot injection). The analysis allowed them to identify best performing conditions. The same research group also used an SRM to investigate a HCCI engine fuelled with hydrogen [27] and ethanol [28] validating their new reduced chemical kinetic schemes. Recently, SRM was also successfully employed to investigate RCCI mode fuelled with n-heptane and iso-octane.

There is little literature on numerical studies of glycerol combustion and, in particular, glycerol–diesel emulsion fuel. This study aims to help fill that gap and demonstrate the use of SRM to simulate complex fuelling in realistic engine conditions. In this paper, engine measurements from the glycerol experimental campaign described in detail by Emberson et al. [15] are adopted and further discussed. Since SRM has proven its accuracy in predictions of combustion processes of various fuels in internal combustion engines, it is a good candidate for being a valuable part of the engine and fuel laboratory. This method was employed in the present study, and its capabilities were further explored. The model calibration procedure was presented based on available experimental data of pressure trace and exhaust emissions. A parametric study was performed to show the sensitivity of the model results to selected model inputs. Owing to the stochastic nature of the model, mixture inhomogeneity was taken into account, and using equivalence ratio–temperature plots, we analysed a time evolution of selected mixture properties under soot-promoting conditions. Interpretation of the results provided insight into the glycerol/diesel combustion process and pollutants formation. The presented results consist of two series for reference diesel and glycerol–diesel emulsion to show the effect of glycerol addition, with particular attention paid to soot formation.

2. Experiment

2.1. Experimental setup

Measurements were conducted in a four-stroke, six-cylinder compression ignition OM 613 Mercedes engine at speed 1800 rpm and different loads. The engine specifications are given in Table 1. Analysed cases considered the engine with turbo charger applied with no EGR, operating in single injection mode. The injection timing was adjusted to provide CA50 at the same location for all the cases, i.e. at ca. 1 CAD after TDC.

PM emissions were collected using a differential mobility spectrometer (Cambustion DMS500) Particle sizes could be measured in the

Table 1
OM 613 Mercedes engine specification.

Number of cylinders	6
Stroke	88.3 mm
Bore	88 mm
Compression ratio	18:1
Displacement volume	3.2 l
Injection system	Mechanical direct

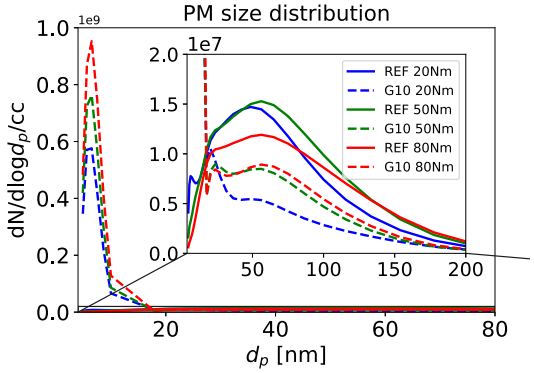

Fig. 1. Particulate matter size distribution for the reference diesel and 10% glycerol emulsion at three different loads.

range of 5 nm to 1 μm. Gaseous emissions were measured with a Horiba Gas Analyser MEXA-ONE-RS, including oxygen, carbon dioxide, carbon monoxide, nitrogen monoxide, nitrogen dioxide (NO_x) and total unburned hydrocarbons (THC).

Two fuels were investigated at loads 20 Nm, 50 Nm, and 80 Nm. For the reference cases, certified diesel fuel was used (EN 590 reference diesel, Coryton Fuels), further referred to as REF. A glycerol emulsion was prepared with 10% (vol) of glycerol, 1% (vol) of surfactant (Span 80 and Tween 80 with a lipophilic–hydrophilic balance of HLB = 6.4), and 89% (vol) reference diesel denoted further as G10. Exhaust gas emission measurements and a combustion pressure trace were used for SRM calibration (shown in Section 4.2). Complete and detailed description of the experimental campaign has been presented previously by Emberson et al. [15].

2.2. Soot measurements

In Fig. 1 particle size distribution (PSD) is presented for the six considered cases. Two main conclusions may be drawn. Firstly, as represented by a dashed lines, glycerol PM emissions are lower than for reference cases for particles larger than 20 nm. However, a high number of small particles with sizes between 4–10 nm is observed, evidenced by a peak of two orders of magnitude higher than that of larger particles. Such a peak is not present in the reference cases at all. A bimodal trend in particle size behaviour has been observed previously for diesel [29–31], heavy-duty natural gas [32] or GDI engines [33], however, the peak of nucleation mode particles was still of the same order of magnitude as the accumulation mode particles and was related to the engine operation rather than the fuel composition effect. In the present case, these particles' origin is believed to have been related to the presence of glycerol [15]. Exhaust particulate emissions were sampled on a glass fibre filter with engine torque of 50 Nm at the particulate matter analyser's location. The reference case sample was black, whereas the colour of the G10 sample was brown. It was concluded that G10 particulate emissions must contain a more significant fraction of non-soot particles, since soot is regarded as black. The large peak of small particles is an issue that has to be considered. If the particles are small solid soot particles, they are especially harmful to human health due to their penetration ability. If however being volatile compounds, they feature enhanced combustion resistance.

In order to determine soot mass concentration, we have employed the concept of effective density, defined as the mass of a particle divided by the volume of a sphere based on the mobility diameter d_m. Maricq and Xu [34] showed that the effective density can be expressed as

$$\rho_e = \rho_0 \left(\frac{d_m}{d_{0e}} \right)^{(d_f - 3)}, \tag{1}$$

where ρ_0 is the primary soot density set to 2 g/cm^3, d_{0e} is an effective primary particle diameter and d_f is the fractal dimension. The two former parameters are selected to fit the experimental data. This approach using $d_f = 2.3$ and $d_{0e} = 20$ nm has also been recently used by, e.g. Kim et al. [35] who analysed characteristics of nanoparticle emission from a light-duty diesel vehicle during test cycles simulating urban rush-hour driving patterns.

The resulting mass concentration distribution is shown in Fig. 2, where the effect of soot reduction is observed. It is clear that the large peak of small particles observed with G10 contributes little to the total soot mass. However, the small difference in the number of the largest particles ($\sim 10^3$ nm) reveals that the G10 produces a greater mass of the largest particles compared to REF fuel. Nevertheless, as shown on the bar plots on the right-hand side of Fig. 2 glycerol addition led to 33%, 45% and 26% total soot mass reduction for 20 Nm, 50 Nm and 80 Nm cases, respectively.

3. Modelling approach

3.1. Stochastic Reactor Model

A challenge in numerical simulations of various combustion processes comes from the complexity of the turbulent flow, chemical reactions and their mutual interactions. Different modelling approaches and simplifications are employed to solve this problem [36]. When focusing on pollutant emissions accurate treatment of chemistry is a priority. Therefore, simulating turbulent reactive flows with the method of transported Probability Density Function (PDF) [37] where the chemical source term does not require modelling is favourable. However, the complex physics of mixing in turbulent flows remains a challenging part to model [38]. Additionally, a tremendous computational cost of 3D CFD calculations, including detailed chemistry, inhibits analysis in practical applications investigating different fuel types and blends. Instead of full-dimensional analysis, a simplified 0D SRM approach developed for the simulations of Internal Combustion (IC) engines can be employed [17]. Due to the dimension reduction of the problem, some IC engine behaviours have to be emulated and calibrated with the aid of experimental data such as combustion in-cylinder pressure trace. However, thanks to the statistical nature of the method, the effects of inhomogeneities and turbulence are still captured. A gas mixture in an engine cylinder in the DI-SRM approach [18] is considered as an ensemble of notional particles which represent a one-point and one-time PDF for a set of scalar variables (species mass fractions and enthalpy). The numerical solution of the PDF equation is obtained using the Monte Carlo method with an operator splitting technique to calculate each submodel equations separately using the LOGEsoft computational code [39].

The composition PDF transport equation excluding radiative heat transfer and spatial derivatives can be written in the following form [37]:

$$\frac{\partial \rho f_\phi}{\partial t} + \frac{\partial}{\partial \Psi_k}\left(\rho S_k f_\phi\right) = \frac{\partial}{\partial \Psi_k}\left(\rho \left\langle \frac{1}{\rho}\frac{\partial J_{k,i}}{\partial x_i} \middle| \Psi \right\rangle f_\phi\right), \tag{2}$$

where f_ϕ is the single-point, joint PDF of species composition and enthalpy (ϕ is the vector of composition variables), Ψ are the sample-space variables corresponding to ϕ, $J_{k,i}$ is the molecular flux of species/enthalpy. On the left-hand side of Eq. (2) the first term is the unsteady rate of change of PDF and the second term represents the change

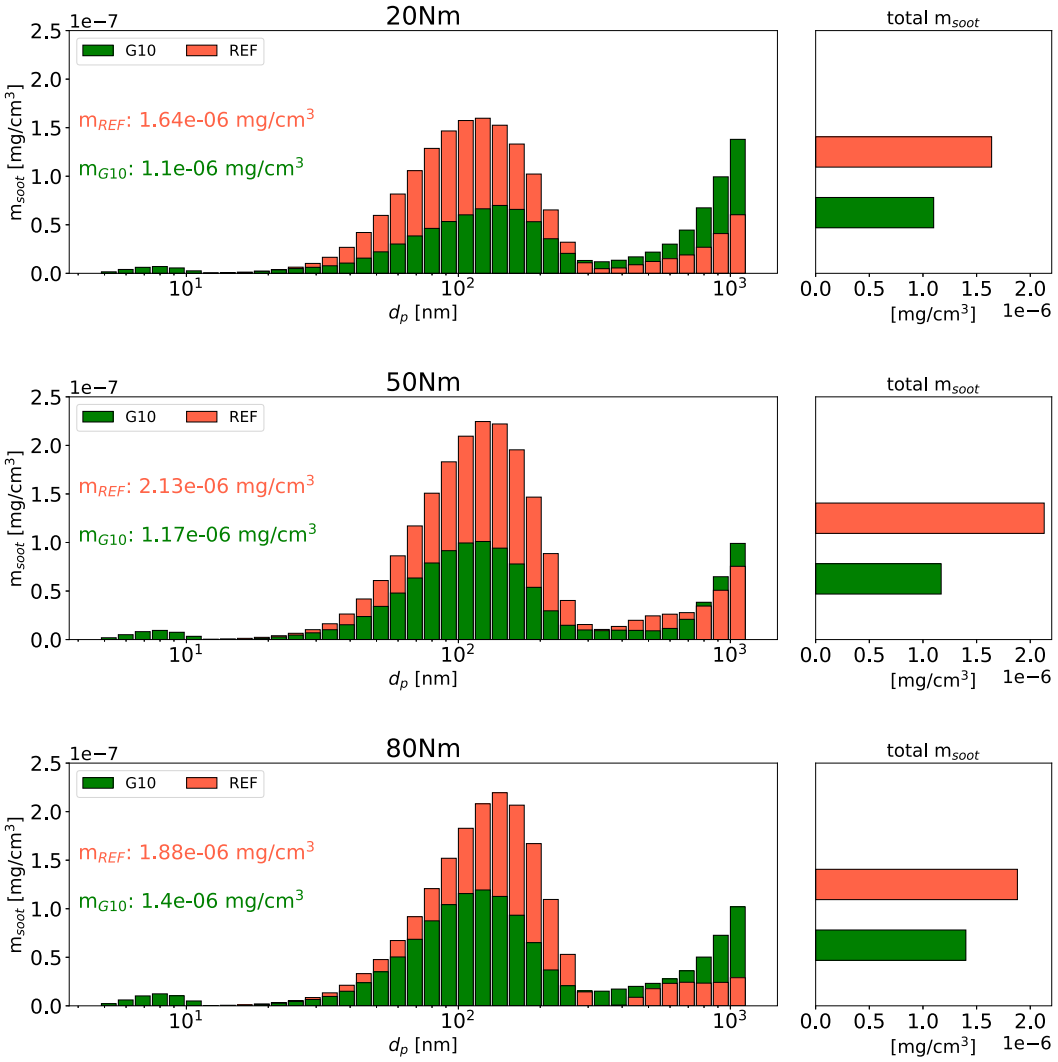

Fig. 2. Particulate matter mass concentration distribution for the reference diesel and 10% glycerol emulsion at three different loads (left). Total PM mass concentration (right).

in composition space by different sources. In the DI-SRM approach, to mimic characteristic engine processes, this term accounts for the volume change due to a piston movement, fuel injections, heat transfer, and chemical reactions [18,23]. The right-hand side term corresponds to molecular mixing and requires modelling closure, usually with the so-called micro-mixing model [38]. The great advantage of this approach is that the chemical source term appears in a closed form and does not require any model. On the other hand, the disadvantage comes when we look at the number of independent variables ($N_\phi + 4$). Due to the high dimensionality of PDF transport equations, solving them in the full space, with, e.g. finite volume method, is impracticable [37]. Therefore, there are several ways to discretize and solve Eq. (2) and can be classified as Lagrangian or Eulerian. In general, the transported PDF methods originated from the work of Pope [40] and an exhaustive review can be found in the work of Haworth [37].

Micro-mixing closure is responsible for appropriate mixing in the composition space. Commonly used models are Interaction by Exchange with the Mean (IEM), Curl mixing or Euclidean Minimum Spanning Tree (EMST) model and are applicable to SRM particle mixing closure. Regardless of the employed approach, the characteristic mixing time scale, understood as a measure of mixing or turbulence intensity is required as an input parameter. It is an ambiguous problem in a zero-dimensional approach; thus, the assistance of, e.g. CFD simulations would be beneficial [41]. Knowing that the level of turbulence changes in time and is different with engine geometry and with engine speed, one can develop simplified approaches to describe this effect. The simplest is to set a single uniform value of mean mixing time as, e.g. in Yasar et al. [24] in conjunction with the localness mixing model (LMM). Korsunovs et al. [21] have used two parameters conversion from turbulence timescale to mixing time scale approach, where one constant was the scaling factor during the injection event and the second one during the rest of the cycle. Pasternak et al. [42] proposed a more elaborated model with parametrized mixing time for the DI-SRM approach, where the model distinguishes between four different phases. Later the model has been assessed and compared against the results from 3D CFD simulations of diesel engine cases showing good performance [19]. Also, Ahmedi et al. [25] adopted the parametrized mixing time model for combustion simulations in a premixed compression ignition (PCI) engine using DI-SRM and three components surrogate model. Recent, and so far, the most realistic model to obtain mixing time in the context of DI-SRM was presented by Franken et al. [20] based on the so-called phenomenological k-ϵ model introduced by Kozuch [43]. The change of the turbulence kinetic energy over crank angle is solved in the following form:

$$\frac{dk}{d\phi} = \left(-C_{den}\frac{2}{3}\frac{k}{V_{cyl}} - C_{diss}\frac{k^{3/2}}{l} + \left[C_{sq}\frac{k_{sq}^{3/2}}{l}\right]_{\phi>TDC} + C_{inj}\frac{dk_{inj}}{dt} + Csw\frac{c_m^3}{l}\right)\frac{1}{6n}, \tag{3}$$

where k is the turbulence kinetic energy, ϕ is the crank angle, V_{cyl} is the instantaneous cylinder volume, c_m^3 is the mean piston velocity, and l is the length scale proportional to the cylinder volume [20]. Parameters C_{den}, C_{diss}, C_{sq}, C_{inj} and C_{sw} have to be calibrated for the considered case and preferably be constant for the same engine. Then, the turbulence time scale is obtained as:

$$\tau = C_\tau \frac{k}{\epsilon}, \tag{4}$$

where C_τ is another scaling parameter and ϵ is calculated as:

$$\epsilon = \frac{dk}{dt} = C_{diss} \frac{k^{3/2}}{l}. \tag{5}$$

Eventually, needed in micro-mixing closure scalar mixing time scale is obtained as:

$$\tau_{mix} = \frac{\tau}{C_\phi}, \tag{6}$$

where C_ϕ is the mixing model constant usually set to 2.0 [20,37]. Finding the six mentioned above parameters is the crucial part of the model calibration and will be presented in Section 4.2.

3.2. Soot modelling

Soot formation in hydrocarbon combustion is the consequence of several local chemical and physical processes. Aromatic rings are rebuilt in the gas phase after the initial decomposition and oxidation of hydrocarbons in rich regions. In chemical models, the reformation of benzene (C_6H_6) can be described using reaction pathways of C_3 [44], and C_4 [45] species in combination with the restructuring of the molecule, also referred to as cyclization [46]. Planar polyaromatic hydrocarbons (PAH) grow mainly via acetylene (C_2H_2) addition from those first aromatic rings. In detailed chemistry models, the growth is described using the hydrogen-abstraction–acetylene-addition (HACA) mechanism [47] with separate ring closure [46]. If hydrogen bonds connect two planar PAH molecules to form a spherical three-dimensional structure, a solid soot nuclei is formed. Soot nuclei can grow further by heterogeneous reactions with C_2H_2 from the gas phase (surface growth), by condensation of further PAH on the nuclei surface, and coagulation with other soot nuclei. After reaching a certain size, the soot particles will agglomerate instead of coagulating. Simultaneously with the growth of PAH and the soot surface, decomposition via oxidation by oxygen (O_2) and OH radicals, as well as the abstraction of C_2H_2 (fragmentation) take place [46]. While the PAH and soot formation occurs in rich regions, the decomposition is located in lean regions. The DI-SRM allows considering this local dependency on equivalence ratio, temperature and available species [19]. Since glycerol is not a common fuel additive, the literature lacks a fully validated reaction mechanism for soot prediction employing glycerol. Therefore, an established benzene ring and PAH growth mechanism [46,48] for the use in Diesel combustion is applied. Crucial species and the impact of the exposure to soot forming conditions are analysed first. C_6H_6 provides information on the potential of PAH growth. C_2H_2 is analysed regarding the potential to contribute to PAH and soot surface growth. The amount of $C_{16}H_{10}$ indicates how many soot particles could be formed since for particle inception or nucleation, the minimum number of aromatic rings is four [49]. The concentration of O_2 and OH is discussed to understand how much of the grown PAH and soot can be oxidized. Next, the detailed kinetic soot model was employed and the results were analysed as well. The Methods of Moments (MoM) from Mauss [46] was used and its implementation in DI-SRM context was presented by Pasternak et al. [19]. Soot source terms were calculated using two soot moments with a fractal dimension of 2.3 [35].

Table 2
Composition of four component surrogate formulation for diesel fuel in mole fractions.

n-hexadecane	0.496
heptamethylnonane	0.257
tetralin	0.176
1-methylnaphthalene	0.061

3.3. Simulation set up

A commonly used surrogate formulation for diesel fuel is n-heptane due to its similarities to real diesel fuels in terms of cetane number (CN) which should ensure similar autoignition behaviour [19]. However, drawbacks of using n-heptane are differences in liquid properties with respect to real diesel and deficiency from not capturing the effects on autoignition and pollutant formation from larger molecules. In this work, we have employed a more accurate surrogate representation consisting of four components: n-hexadecane, heptamethylnonane, tetralin, and 1-methylnaphthalene (see Table 2) obtained with analogous methodology as presented in [50]. In many previous SRM studies on diesel fuels [19,20,23] the mechanism given by Seidel et al. [51] proved to provide satisfactory results. It consists of 56 species and 206 reactions and is dedicated to n-heptane combustion. This mechanism provides a good compromise between chemical complexity and computational effort required in 0D SRM simulations. However, the mentioned mechanism does not contain glycerol kinetics and all components from the selected surrogate formulation. Jach et al. [13] pointed out that the glycerol properties make it challenging to pursue experiments in a shock tube or rapid compression machine, thus literature lacks this type of data. Therefore, there is not many chemical kinetics for glycerol combustion, so we chose a complete chemical mechanism for the combustion of hydrocarbon and oxygenated fuels from Ranzi et al. [52], which includes 484 species and 19341 reactions. The employed glycerol part of the chemical mechanism has been validated for experiments with glycerol pyrolysis [53], and combustion of propanol–glycerol mixture droplets under reduced-gravity from Dee and Shaw [54].

As mentioned earlier, in 0D SRM simulations, critical in-cylinder processes included in the PDF equation have to be emulated or modelled. Volume change due to a piston movement is straightforward and depends on the engine speed and geometry. Heat transfer to the wall was calculated with the Woschni's model. Fuel injection was simplified in this study by injecting fuel in a gaseous phase with injection time adjusted to match a heat release rate slope. For micromixing closure for particle interactions, the EMST model was used, which accounts for localness mixing criteria in the sense that particles with similar properties (neighbours in the scalar space) can interact with each other. The comparison with simpler Curl mixing model made by Franken et al. [20] has shown that EMST provided much more realistic results in heat release rate and scatter data in T-ϕ map. Micro-mixing depends on turbulent mixing time, and its modelling in 0D simulation remains the most challenging part of the SRM approach.

In this work, we have employed the 0D k-ϵ model adjusted to the SRM simulations to obtain more physical mixing time profiles than often applied in simplified approaches when mixing time is constant or manually constructed based on specified parameters. This model is dependent on five constants, which should be calibrated for the investigated engine and are kept the same for all operating conditions. These constants determine the k solution obtained with Eq. (3) and thus the shape of the mixing time profile. The mixing time optimization process was performed using 200 particles, CAD time step set to 0.5 and just one engine cycle. Table 3 presents the final calibrated DI-SRM model setup parameters where 20 engine cycles were simulated with the number of stochastic particles increased to 1000. Both optimization and analysis were performed employing online chemical kinetics calculations without tabulation. Sensitivity analysis for the turbulence model

Table 3
DI-SRM model setup during optimization[(a)] and full run[(b)].

Mixing model	1D EMST
Number of particles	200[(a)]/1000[(b)]
Number of cycles	1[(a)]/20[(b)]
Time step size [degCA]	0.5
Heat transfer model	Woschni
Woschni C_1	2.28
Woschni C_2	0.0035

constants is presented in Appendix. A relatively small change in the results due to the modifications also indicates a satisfactory calibration process. Recently, Korsunov et al. [21] performed the analysis aiming for an optimal trade-off between the NO_x emissions and physical in-cylinder measurements accuracy, pointing out critical sensitivity to the input parameters and modelling conditions. We can confirm this observation, and the impact of initial pressure, temperature, injected fuel mass, injection timing, and the level of internal EGR was assessed, and the results are included in the sensitivity analysis in Appendix.

4. Numerical results

4.1. Constant pressure reactor simulations

At first constant pressure reactor simulations have been performed to investigate the effect of chemical kinetics. Several cases, corresponding to the given in-cylinder engine conditions have been simulated and the results of CO as well as C_2H_2 as a soot precursor have been compared between the reference diesel and G10 emulsion. A similar chemical kinetics study under relevant conditions showing the effect of glycerol addition on the missions has been presented previously in [15]. They have employed n-heptane as a diesel surrogate and used different chemical schemes and reported a small increase in CO and a decrease in selected soot precursors. The glycerol addition did not influence the emissions dramatically and as shown by the results presented in Figs. 3–4 changes in equivalence ratio, temperature or pressure conditions can alter the results to a larger extent than the fuel composition. At higher temperatures the effect of equivalence ratio and pressure is much stronger than the chemical. However, at lower temperatures (see $\phi = 0.25$ and$T = 800$ K) the chemical effect can be comparable to the change in pressure of few bars.

4.2. SRM calibration

A number of simulations have been performed to carry out the SRM calibration procedure [20]. The priority was to find the same set of turbulence model parameters for all loads, matching experimental pressure traces. Only C_{inj} parameter determining minimum value of the mixing time had to be adjusted in every case to properly capture the pressure peak, yet having a minimal impact on the mixing time profile shape (see Fig. 7 right). The final set of parameters used in the k-ϵ turbulence model are shown in Table 4. Comparison of numerical results and experimental data used for calibration is presented in Fig. 5 showing good agreement for all considered cases. Additionally, in Fig. 6 experimental and numerical data of heat release rate are presented for each load comparing the two fuels, where it can be observed that G10 results are characterized with later ignition than the REF case. The experimental peaks of the heat release rate are higher for G10, and the profiles drop simultaneously as for the REF cases that indicate shorter combustion phasing. Similar observation can be made comparing the SRM RoHR profiles with the restriction that the numerical peak values are slightly lower than the experimental ones, and for medium and high loads, G10 peaks are at the same level as in the REF cases. Fig. 7 shows comparison of the temperature, pressure and mixing time scale results obtained with SRM for the two fuels at three different

Table 4
Final calibrated DI-SRM turbulence model parameters.

Parameter	C_{den}	C_{diss}	C_{sq}	C_{inj}	C_{sw}	C_{τ}
Value	1.5	2.0	1.0	2.4–18.0	8.0	0.5

loads. It is noticeable that the maximum pressures and temperatures are higher for glycerol cases at the same load. This effect is also observed for experimental pressures, that can be a consequence of the higher injected mass of G10 emulsion. Available temperature profiles are obtained numerically only, and the maximum values are higher for the G10 cases but shortly after reaching the peak, the temperature drops slightly below the temperature for the reference diesel cases. Looking at the exhaust emissions shown in Fig. 8, measured NO_x values are approximately at the same level for both REF and G10 fuels, whereas numerical values indicate higher NO_x emissions for G10, that can be linked to the higher maximum temperatures. Otherwise the trend in NO_x emissions was captured very well. From previous research on glycerol emulsion combustion in CI engine conditions, it is expected that glycerol addition will result in incomplete combustion [7,12,15]. Consequently, an increase in CO emissions is expected, most evident at low load conditions as shown in the experimental data in Fig. 8 (bottom left). This trend is not captured by the SRM model, and as shown in Fig. 3, it is also not dependent on the chemical kinetics. Sidhu et al. [7] pointed out that the higher viscosity of glycerol can reduce the fuel spray atomization and consequently increase the CO emissions. The model used here does not account for the fuel spray and atomization, which can explain why the effect of increased CO emissions with G10 was not captured. Major species emissions i.e. O_2 and CO_2 were predicted with good agreement to the experimental data.

4.3. Soot predictions

The SRM has a significant advantage over, other 0D models in that it accounts for scalar inhomogeneities in the in-cylinder gas mixture. For each stochastic particle at each time step, scalar values can be shown in the scatter plots representing the inhomogeneous mixture to identify conditions promoting pollutant emissions, i.e., NO_x or soot. T-ϕ maps analysis, similar of that based upon 3D CFD simulations can be presented [55], but with possibility to use a much larger chemical mechanism. Fig. 9 shows scatter plots of temperature and equivalence ratio values in stochastic particles between −5 CAD to 15 CAD aTDC for a representative simulation cycle. In the figures, results of REF and G10 emulsion are compared for the three loads. The shaded area indicates the soot formation region. To identify how many and for how long the particles reside in the soot region, the plots in Fig. 10 present the number of particles in the soot region plotted over time. Each symbol represents a stochastic particle with a given index (which counts particles from the soot region) at a given time step. The top plots show the count of particles in the soot region for each time step. Thus, for example, we can learn from the plot for 20 Nm case that for the fuel REF, the particle with the index “0” stays in the soot region for three time steps from −1.0 CAD to 0 CAD aTDC and that at the time of −1.0 CAD aTDC there are 15 particles in the soot region for REF fuel and none for G10 fuel. All the plots indicate that with increased load more significant fraction of in-cylinder gas, indicated by a larger number of particles, passes through the soot promoting region. For all loads, the total number of particles with equivalence ratio and temperature relevant for the soot production is larger for the REF fuel than for the G10 cases. At the same time, we can see that for the G10 cases, particles enter the soot region with some delay with respect to the REF case and stay there for a shorter period. This behaviour correlates with longer ignition delay time and shorter combustion phasing observed by comparing the rate of heat release between REF and G10 shown in Fig. 6.

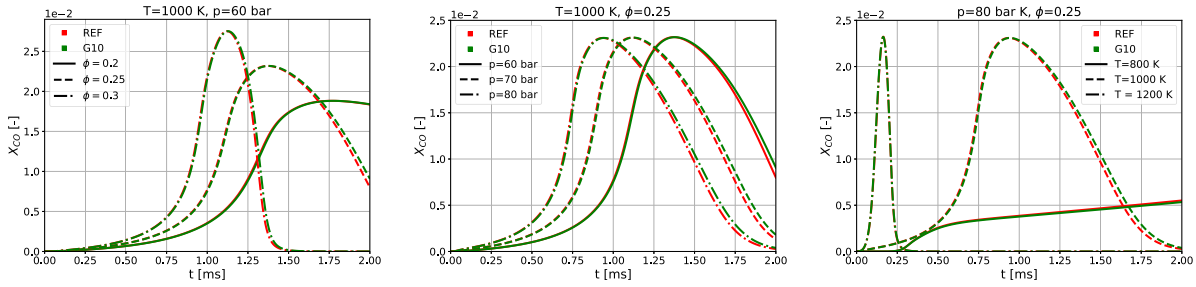

Fig. 3. Results from chemical kinetic simulations performed for constant pressure reactor at different conditions. Plots shows mole fraction of CO, where red lines represent simulation results from mixture of reference diesel, whereas the green lines represents 10% glycerol mixture. (For interpretation of the references to colour in this figure legend, the reader is referred to the web version of this article.)

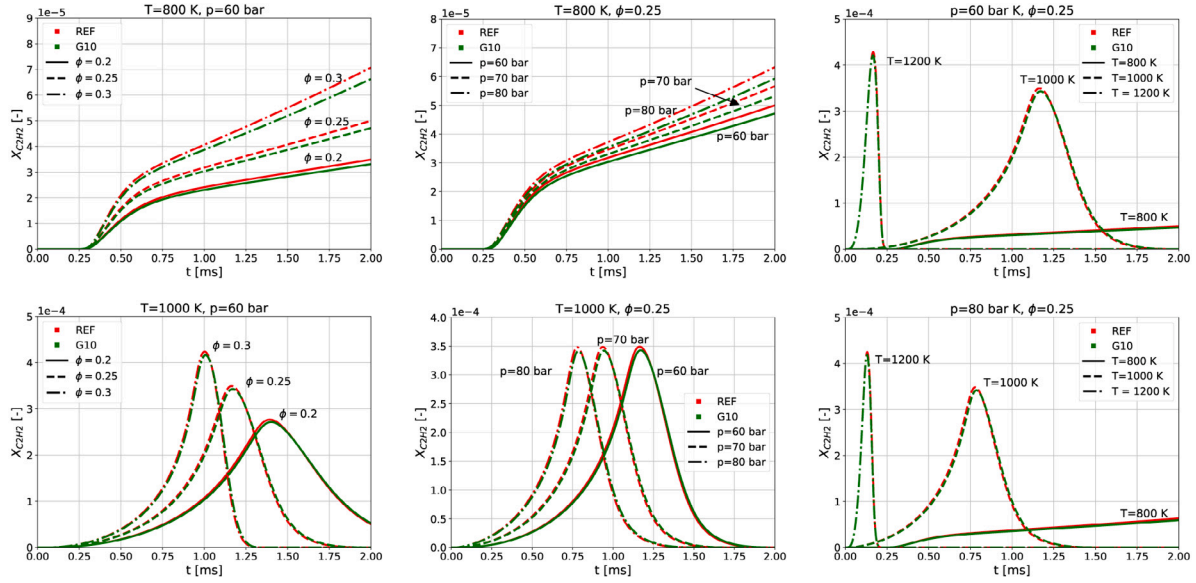

Fig. 4. Results from chemical kinetic simulations performed for constant pressure reactor at different conditions. Plots shows mole fraction of C_2H_2, where red lines represent simulation results from mixture of reference diesel, whereas the green lines represents 10% glycerol mixture. (For interpretation of the references to colour in this figure legend, the reader is referred to the web version of this article.)

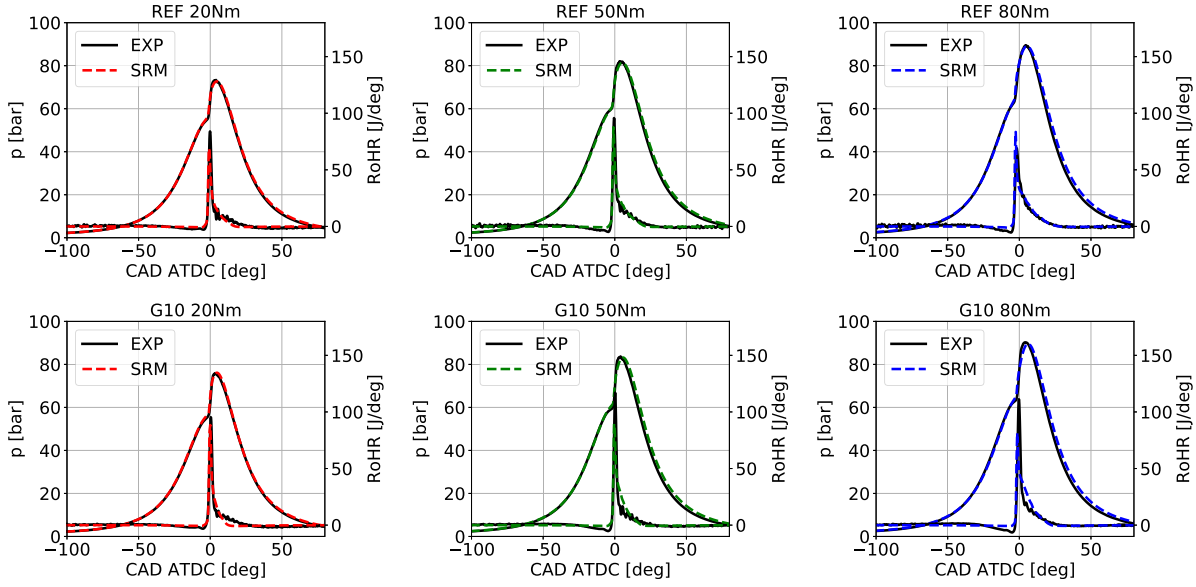

Fig. 5. Comparison of experimental and DI-SRM simulation cylinder pressure and heat release rate for reference diesel and glycerol emulsion fuelled cases at three loads 20 Nm, 50 Nm, 80 Nm.

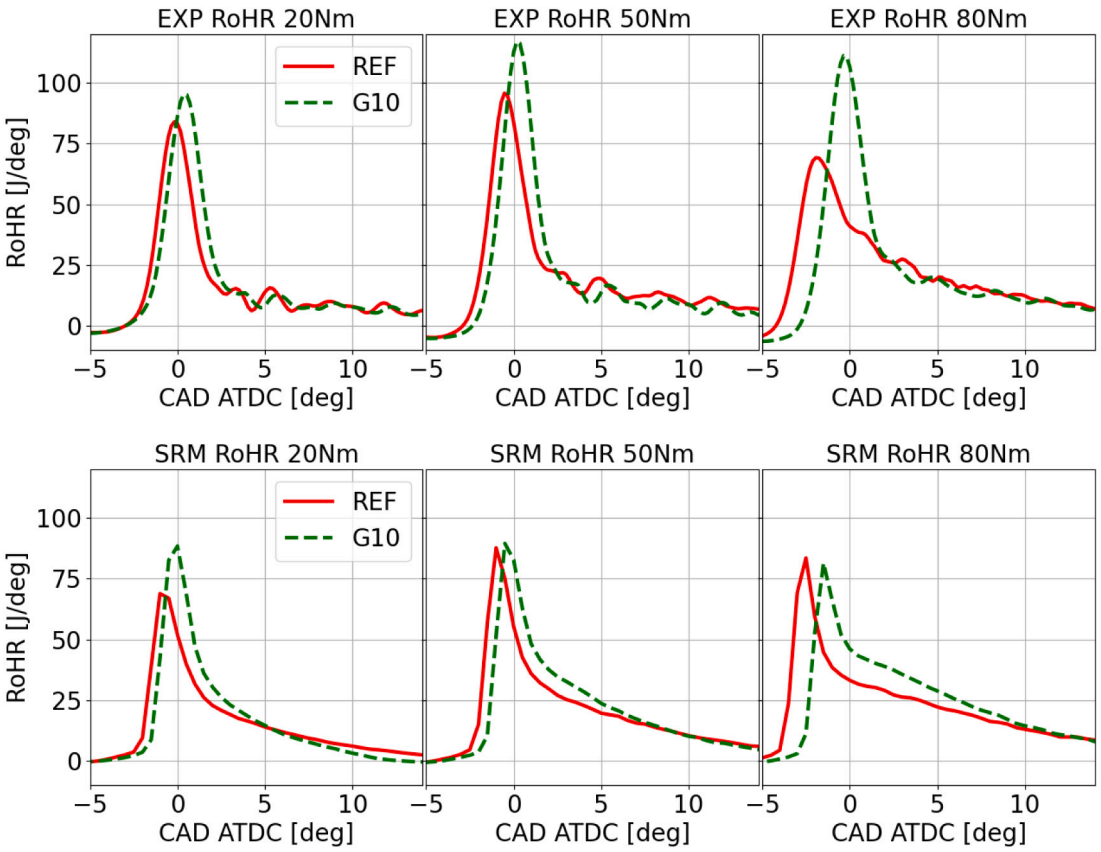

Fig. 6. Comparison of the experimental (top row) and numerical (bottom row) heat release rates between the two fuels for each load.

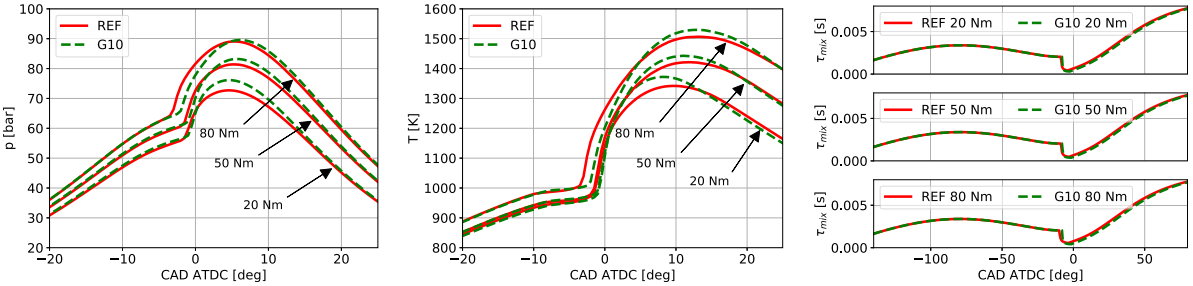

Fig. 7. Comparison of the pressure, temperature and mixing time for the REF and G10 fuels at the three different loads.

The shorter combustion phasing is also visible in the concentration of selected species time evolution shown in Fig. 11 in the units of parts per million (molar based). Solid red lines denote total concentrations for REF cases, whereas dashed lines represent concentrations of selected species counting only the particles from the soot region. Similarly, dashed–dotted green lines represent G10 cases counting the total concentration, whereas dotted lines show the respective concentrations only for the soot region particles. It is prominent that nearly all available C_2H_2 soot precursor is present in the particles under soot promoting conditions. We can see that the C_2H_2 peak value is always lower for G10 emulsion than for REF fuel, but the difference is smaller for higher loads. Simultaneously, the period where these soot precursors are present is slightly shorter for cases fuelled with G10. Concentrations of the hydroxyl radical known as soot oxidizer are presented in the second row in Fig. 11. For the low load case (20 Nm), the total OH concentration peak is distinctly higher for G10 emulsion than for REF fuel, but in the soot region, the OH peaks for the two fuels are at the same level for all loads. It is interesting to note that for G10 cases, the total concentration of OH in all the particles starts to increase later than for REF cases but it peaks earlier. Moreover, in the particles which were in the soot favourable conditions, OH concentrations grow and peak earlier than for REF cases. The total concentration of oxygen over time in all the particles is very similar for both fuels. Some variations of O_2 concentrations can be observed in the "sooting" particles shown in the bottom row of Fig. 11, where O_2 drops to zero during the intense period of combustion for both fuels, but for G10 it starts to increase earlier and is higher until 40–60 CAD aTDC. However, it should be pointed out that after 10 CAD aTDC none of the particles remains in the soot favourable conditions, and the majority of the in-flame soot is already oxidized, which will be shown in Fig. 12.

Fig. 12 shows soot mass formation and destruction rates. Soot formation mechanisms concerns nucleation, condensation and surface growth. The process of soot coagulation and agglomeration are considered, but they contribute to the number of soot particles and do not change the total soot mass, so it is not presented. Peaks of formation rates due to surface growth and condensation for both fuels at 20 Nm load are almost at the same level, whereas for the medium and high loads, they are slightly larger for the G10 emulsion. The nucleation

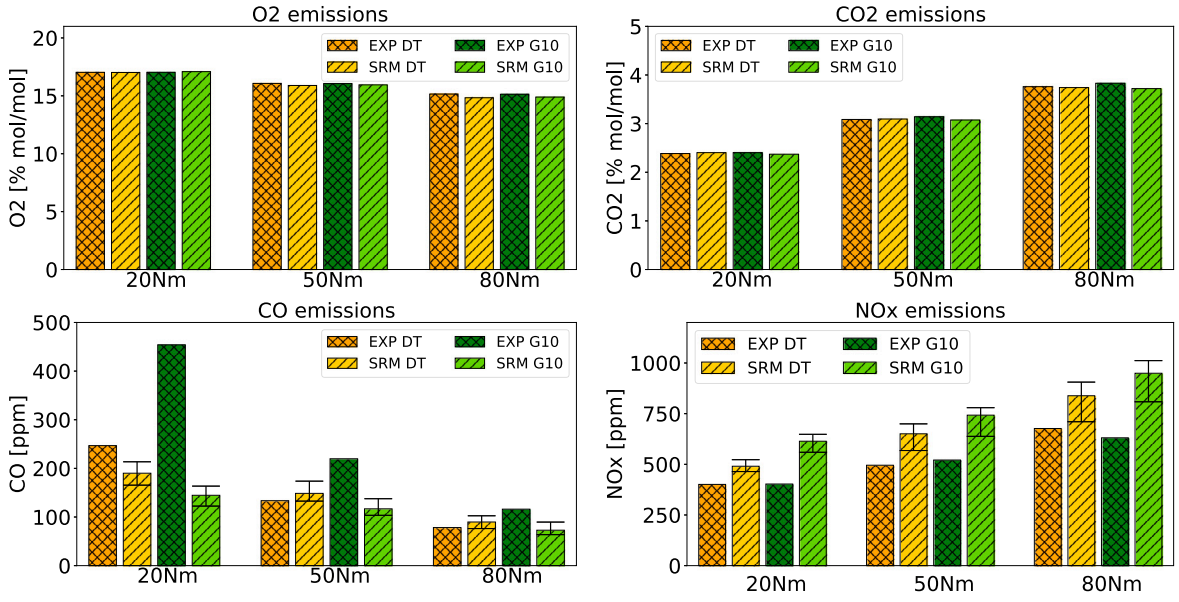

Fig. 8. Exhaust emissions of O_2, CO_2, CO and NO_x emissions. Experimental measurements for the three loads fuelled with the reference diesel and glycerol emulsion are compared with numerical SRM results and presented as mean values over twenty cycles. Error bars in CO and NO_x numerical results denote maximum and minimum values over all the cycles.

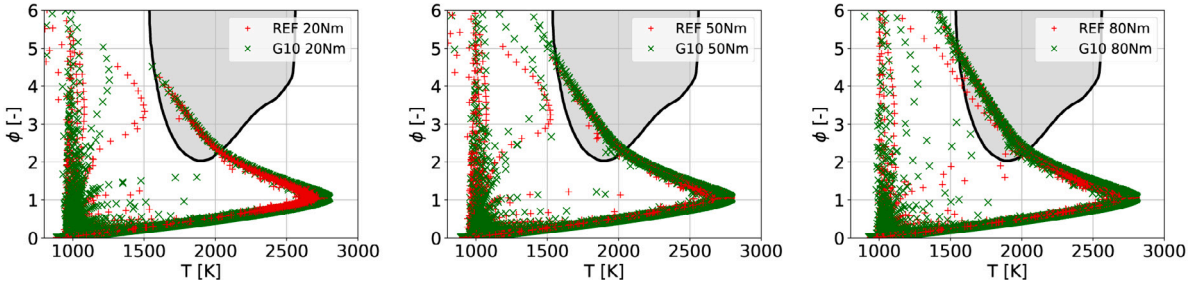

Fig. 9. Scatter plots representing equivalence ratio and the temperature for each stochastic particle between −5 CAD to 15 CAD aTDC for REF and G10 cases.

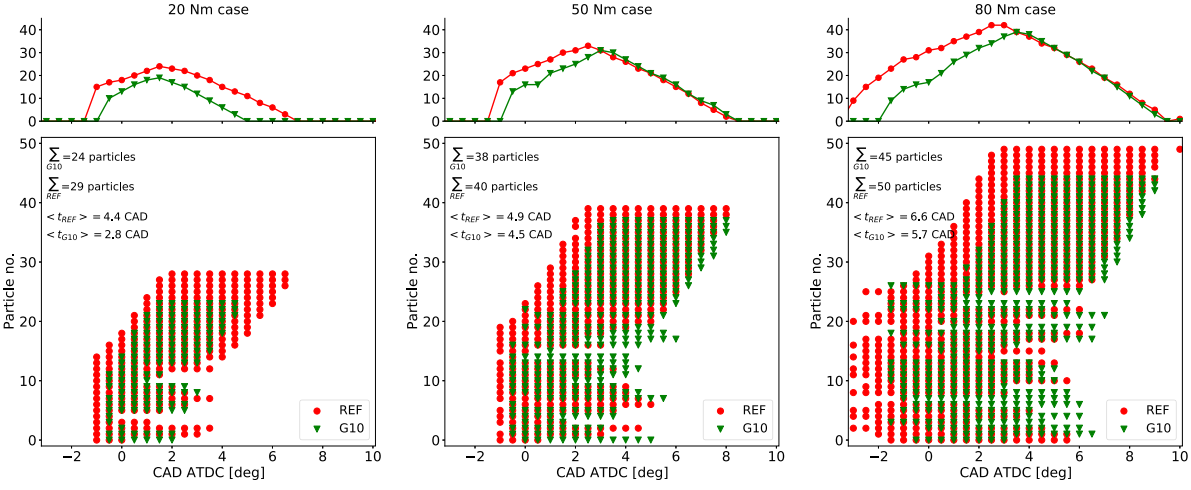

Fig. 10. Count of stochastic particles residing in the soot production region shown in the T-ϕ map at each time step for the two fuels.

rate peak at high load is twice as high for REF case as for G10, but they are at the same level for the two lower load conditions. The nucleation peak of the REF fuel is always earlier than for G10, which correspond to the longer effective ignition delay time observed experimentally [15]. Peaks of surface growth and condensation rates correlate well with peaks of PAHs (A3R5- or A3R5) and acetylene (C_2H_2), which is related to the surface growth mechanisms driven by the hydrogen abstraction acetylene addition (HACA) [47] with a separate ring closure (HACARC) [46]. Similar observations can be made for the destruction rates, where soot oxidation due to heterogeneous reactions with molecular oxygen is the same for the two fuels for all loads and oxidation with the hydroxyl radical is higher with G10 at medium

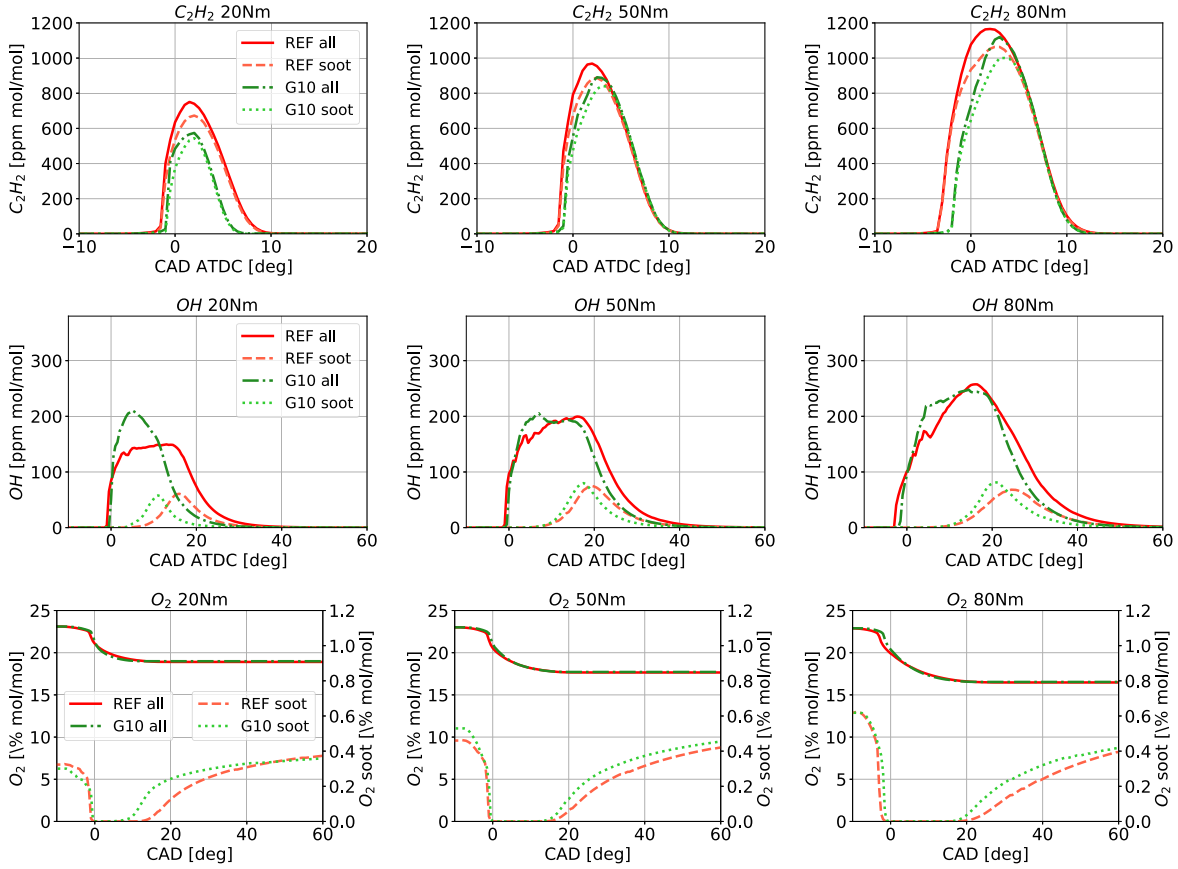

Fig. 11. Concentration in parts per million (molar based) of C_2H_2, OH and O_2 for the two investigated fuels and the three loads. Data series denoted with "all" consider concentration over all stochastic particles, whereas data series denoted with "soot" consider concentrations calculated for the particles, which were in the soot favourable conditions.

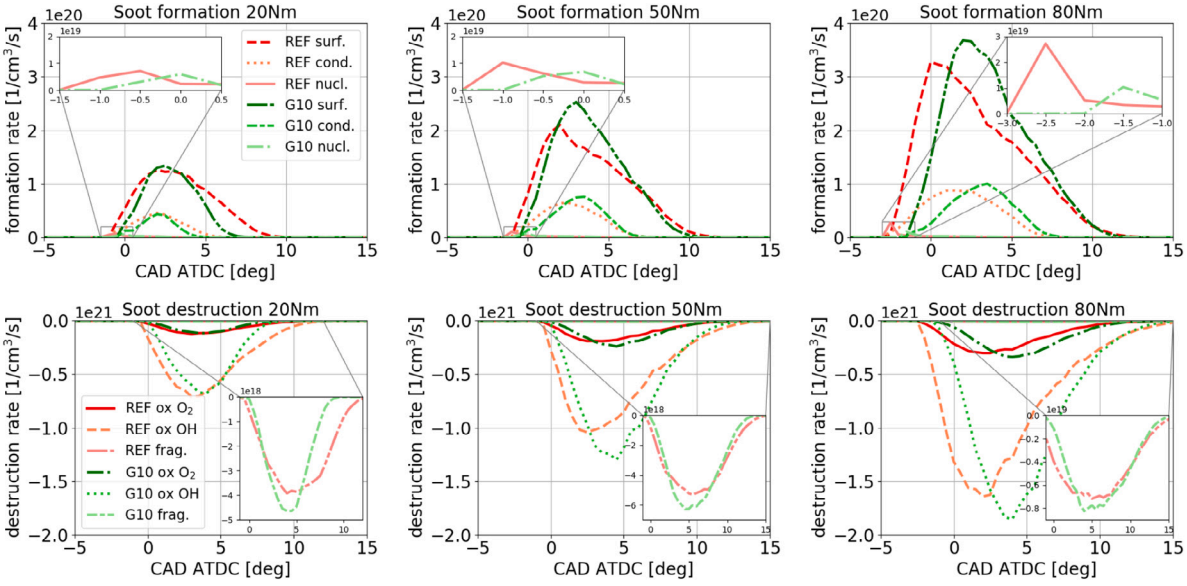

Fig. 12. Mean soot formation and destruction rates for the two fuels and three loads. Soot formation is accounted by nucleation (zoomed inset) surface growth and condensation. Destruction rates are composed of oxidation with OH, O_2 and fragmentation (zoomed inset).

and high loads. Fragmentation, which is a soot destruction process of abstracting an acetylene molecule from the soot surface whose rate is three order of magnitude lower than the oxidation processes, as shown in the zoomed inset in Fig. 12 (bottom row), is slightly higher for G10 at all loads.

Fig. 13 shows the comparison of mean soot mass fraction distribution in the period between −5 CAD and 15 CAD aTDC for the REF fuel and G10 at three different loads. Clearly, for all the conditions at any time, the mean mass fraction of soot is lower for the fuel with glycerol added. Also, the maximum soot mass fraction is higher for higher load,

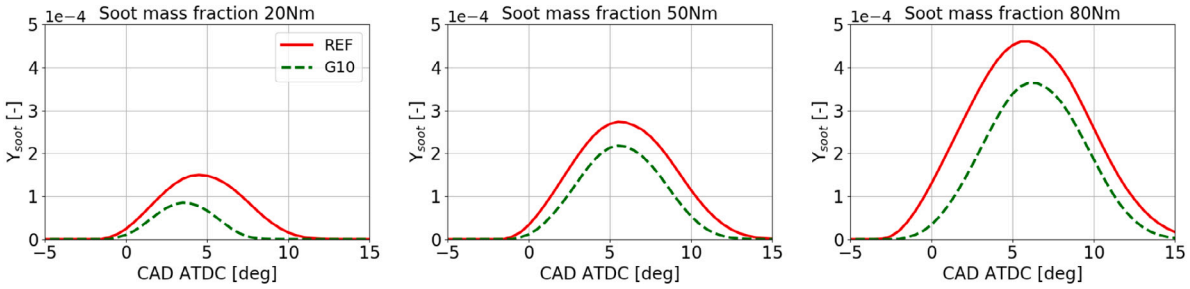

Fig. 13. Soot mass fraction evolution in time between −5 CAD and 15 CAD aTDC for the two investigated fuels and three loads.

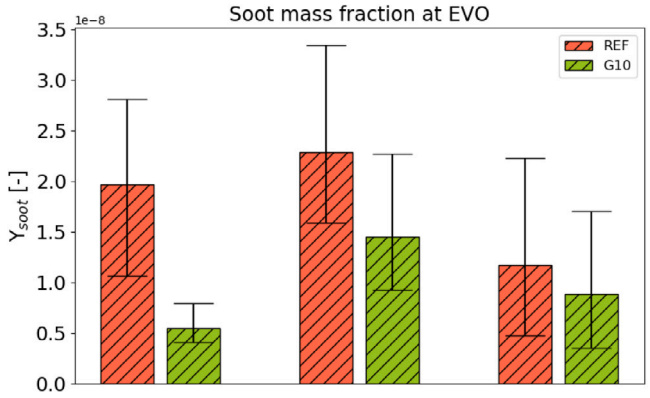

Fig. 14. Soot mass fraction at the EVO averaged over 20 cycles for the REF and G10 fuels and three loads. Error bars denote maximum and minimum values over all the cycles.

which correspond to the amount of mass present in the soot production region shown in Fig. 10 at different loads. However, as presented in Fig. 14 this tendency is not sustained for the emissions at the EVO, and the values do not follow any specific trend correlated with the load, which is in agreement with the experimental observation shown in Fig. 2. The majority of the produced soot is oxidized, but the effect of soot reduction with the use of glycerol is still evident. The highest decrease in soot is observed for the low load, and for medium and high loads some overlapping in error bars is present. The error bars mark maximum and minimum mass fractions of soot at EVO during a single cycle, and they indicate relatively large cycle-to-cycle variations in soot predictions. All the results indicate that shorter combustion phasing and lower mass fraction resided in the soot promoting region for the glycerol cases played the major role in the soot reduction. However, for the low load case, the soot precursors C_2H_2 were clearly at lower level and hydroxyl radical concentration was at higher level for G10 compared to the reference diesel fuel case. This observation can explain much higher soot reduction effect for the low load with respect to medium and high load where the level of ethylene and hydroxyl radical were very similar for the two fuels.

The employed soot MoM model does not predict PSD, thus is not able to directly reproduce the data shown in Fig. 1 and explain the nature of the large number of small size soot particles that were found for G10 emulsion. Soot sectional method [56] would be better suited to attempt that goal. Nevertheless, analysing the present soot model results, such as nucleation rates, could provide some helpful information on differences in the soot production and destruction mechanisms, yet it did not provide any evidence for the origin of the smallest particles. On the other hand, comparing the ratios of mass fractions of the same species between G10 and REF for the relevant loads, it was found that besides unburned glycerol, its oxidation intermediate products such as acetol and 3-hydroxypropanal were present in the exhaust only for G10 emulsion. Their boiling points are above or close to the exhaust gas temperature (~ 440 K), thus they could condense and be detected by the experimental equipment as tiny particles. This observation aligns with the previous hypothesis supported by TGA analysis [15] of the soot collected on a filter that the semi-volatile organic compounds have started to condense, leading to the peak of sub 10 nm particles absent in the pure diesel cases.

5. Conclusions

Numerical simulations using detailed chemistry to model multi-component diesel fuel surrogate and its emulsion with glycerol have been performed using the Stochastic Reactor Model. This simulation tool appears as an attractive method to gain deeper understanding of the combustion process in realistic DICI engine conditions. The model capabilities have been shown based on pollutants emissions and soot formation analysis, and major findings are the following:

- The SRM model was calibrated to the pressure trace using a robust method based on machine learning algorithm and optimization loop;
- Increase in CO emissions for glycerol emulsion was not captured by the SRM model, which indicates that the explanation of this behaviour is in the underlying physics of spray and mixture formation rather than related to the chemical effect;
- Differences in thermodynamic and physical conditions were identified as a more dominant factor to trigger pollutants emissions and soot formation than the glycerol chemistry;
- The soot reducing effect of glycerol was confirmed numerically and was mainly related to the shorter period of combustion process;
- A similar level of soot precursors and oxidizers were observed for both fuels at medium and high loads, whereas at low load less ethylene and more hydroxyl radical were produced, which resulted in enhanced soot reduction obtained numerically with G10. This observation indicates that shorter combustion phasing alone was a sufficient factor in reducing the soot to the comparable level as achieved in the experiment.
- Quantitative conclusions from the results of soot production and formation rates showing minor differences between the two fuels should be drawn with some circumspection due to the sensitivity of soot model prediction to the majority of input parameters (see Appendix);
- Soot model results did not provide any evidence for the origin of a large number of small-sized soot particles present in G10 PSD measured in the experiment. It was pointed out that unburned glycerol and its oxidation intermediate products could condense and be measured as tiny particles.
- In the sensitivity analysis, it has been shown that the model is essentially sensitive to selected input parameters. It is of high importance to pay attention to accuracy and precision during experimental measurements of those parameters. It is expected that employing simple CFD analysis to derive a mixing time scale could significantly reduce the number of parameters, which poses difficulties in finding their optimal set.

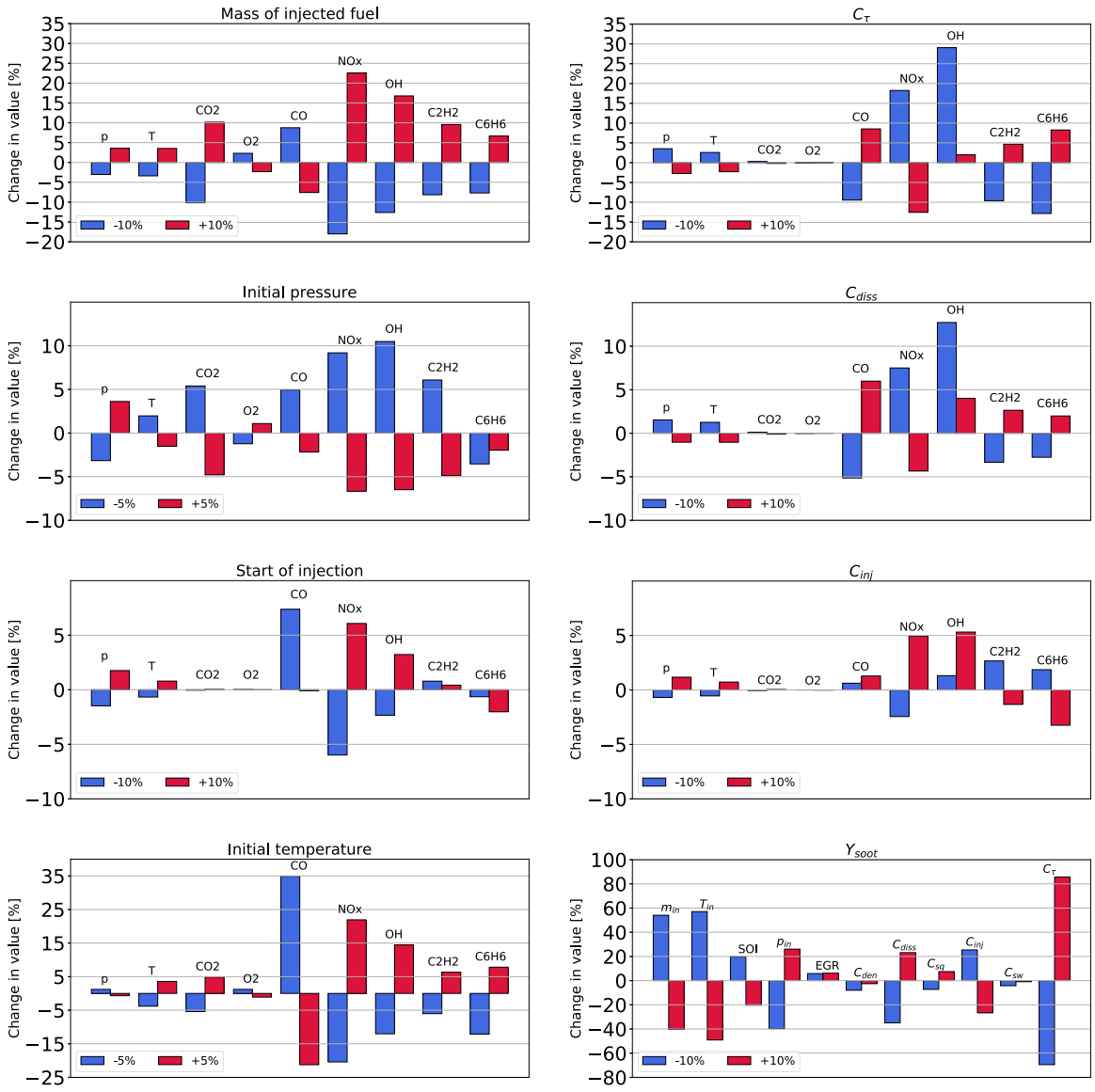

Fig. 15. Relative change in value (mean values over 20 cycles) of selected model outputs as a result of ±5% or ±10%, change in selected inputs. Note that the relative change of the soot mass fraction is presented in a separate figure (bottom right) due to its high sensitivity.

CRediT authorship contribution statement

Michał T. Lewandowski: Investigation, Conceptualization, Methodology, Software, Visualization, Validation, Formal analysis, Writing – original draft. **Corinna Netzer:** Conceptualization, Software, Writing – review & editing. **David R. Emberson:** Investigation, Resources, Writing – review & editing. **Terese Løvås:** Writing – review & editing, Supervision, Project administration, Funding acquisition.

Declaration of competing interest

The authors declare that they have no known competing financial interests or personal relationships that could have appeared to influence the work reported in this paper.

Acknowledgements

The research has been supported by the research centre Bio4fuels, which is part of Centres for Environment-friendly Energy Research (FME) funded by the Norwegian Research Council. We are thankful to dr. Ahfaz Ahmed at Chalmers University of Technology for the discussion on the diesel fuel surrogate formulation and Jan Wyndorps (RWTH Aachen) for discussion on the experimental set-up. The computations were performed on resources provided by the NTNU IDUN/EPIC computing cluster. LOGE AB is acknowledged for providing the licence for the LOGE Research software.

Appendix. SRM sensitivity

Sensitivity to eleven selected model parameters and engine initial conditions is presented here. Change ±5% in initial temperature and pressure values and ±10% change in start of injection, injected fuel mass, and $k-\epsilon$ turbulence model parameters (C_{diss}, C_{inj}, C_τ) and the results are presented in Fig. 15. The impact of ± 10% change in EGR, C_{den}, C_{sw} and C_{sq} values was assessed as well but was lower than 2%–3% for any of the studied quantity and thus is not shown. The results in Fig. 15 show the change in value of selected quantity with respect to the simulation result obtained with optimal set of parameters ($e = 100 \times (y_{opt} - y_{\pm 5/10})/y_{opt}$). The assessed quantities of interest were outlet CO_2, O_2, CO, NO_x, soot and peak values of temperature, pressure, OH, C_2H_2, C_6H_6 The case at 20 Nm load fuelled with the reference diesel was considered for that purpose. In-cylinder initial temperature

after IVC is difficult to measure and it has to be estimated based on the measured pressure and the measured air mass flux (to match the pressure curve during compression), it is observed to have a large impact on the combustion simulation results. The mass of the fuel injected into the cylinder during the injection can be measured with limited accuracy in the experimental set-up used here and is another critical parameter that strongly influences the simulation results.

In the present work the level of in-cylinder turbulence is predicted using one-equation model for mean turbulence kinetic energy which consequently provides the mixing time profile needed in micro-mixing closure. Previously, until the work of Franken et al. [20], no turbulence model behind mixing time profile was present. During the process of optimization using mentioned $k-\epsilon$ model one has to calibrate 6 model constants, which determine the k solution and thus the shape of the mixing time profile. Influence of these constants can be regarded as the sensitivity analysis on the effect of turbulence model. Achieving, small changes in the monitored values, can be also understood as an indicator of the model convergence. The parameter C_τ has the strongest effect on the assessed quantities because it multiplicates the value of mixing time in the whole range from IVC to EVO. It moves the mixing time, shown in Fig. 7 up or down. The parameter C_{inj} triggers the effect of enhanced mixing due to fuel injection, which can influence the peak pressure and temperature but has also impact on the emissions. Other $k-\epsilon$ parameters are responsible for the mixing time shape evolution due to density change, swirl motion and squish flow [20]. Simulation results were found to be weakly sensitive with respect to changes in values of C_{sw} and C_{sq}. C_{den} and C_{diss} were found to be much more important, however within ±10% around the optimized value, a change in C_{den} had a marginal impact. Among the monitored model outputs, soot mass fraction is the most sensitive, and therefore is presented in the separate plot (bottom right) in Fig. 15.

Definitions/abbreviations

DICI — Direct Injection Compression Ignition
PM — Particulate matter
PSD — Particle size distribution
MoM - Method of Moments
CFD — Computational fluid dynamics
SRM — Stochastic reactor model
PDF — Probability density function
IEM — Exchange with the mean
EMST — Euclidean Minimum Spanning Tree
CN — Cetane number
LHV — Lower heating value
EGR — Exhaust gas recirculation
TDC — Top dead centre
ATDC — After top dead centre
CAD — Crank angle degree
DI-SRM — Direct injection stochastic reactor model
SOI — Start of injection
EVO — Exhaust valve opening
IVC — Inlet valve closure
PAH — Polycyclic aromatic hydrocarbon
TGA — Thermogravimetric analysis

References

[1] Shirvani S, Shirvani S, Reitz R, Salehi F. Thermodynamic energy and exergy analysis of low-temperature combustion strategies. SAE Int J Eng 2021;14:03–14–03–0021.
[2] Khalife E, Tabatabaei M, Demirbas A, Aghbashlo M. Impacts of additives on performance and emission characteristics of diesel engines during steady state operation. Prog Energy Combust Sci 2016;59:32–78.
[3] Chen Z, Sun W, Zhao L. Combustion mechanisms and kinetics of fuel additives: A reaxff molecular simulation. Energy Fuels 2018;32:11852–63.
[4] Lapuerta M, Armas O, Rodr'iguez-Fern'andez J. Effect of biodiesel fuels on diesel engine emissions. Prog Energy Combust Sci 2003;34:198–223.
[5] Rounce P, Tsolakis A, Leung P, York APE. A comparison of diesel and biodiesel emissions using dimethyl carbonate as an oxygenated additive. Energy Fuels 2010;24:4812–9.
[6] Kozak M, Merkisz J, Bielaczyc P, Szczotka A. The influence of oxygenated diesel fuels on a diesel vehicle PM/NOx emission trade-off. SAE Technical Paper, 2009-01-2696, 2009.
[7] Sidhu MS, Roy MM, Wang W. Glycerine emulsions of diesel-biodiesel blends and their performance and emissions in a diesel engine. Appl Energy 2018;230:148–59.
[8] Bohon MD, Metzger BA, Linak WP, King CJ, Roberts WL. Glycerol combustion and emissions. Proc Combust Inst 2011;33:2717–24.
[9] Leung Dennis YC, Wu Xuan, Leung MKH. A review on biodiesel production using catalyzed transesterification. Appl Energy 2010;87(4).
[10] Quispe César AG, Coronado Christian JR, Carvalho João A Jr. Glycerol: Production, consumption, prices, characterization and new trends in combustion. Renew Sustain Energy Rev 2013;27:475–93.
[11] Nda-Umar UI, Ramli I, Taufiq-Yap YH, Muhamad EN. An overview of recent research in the conversion of glycerol into biofuels, fuel additives and other bio-based chemicals. Catalysts 2019;9:15.
[12] Eaton SJ, Harakas GN, Kimball RW, Smith JA, Pilot KA, Kuflik MT, et al. Formulation and combustion of glycerol–diesel fuel emulsions. Energy Fuels 2014;28:3940–7.
[13] Jach A, Cieślak I, Teodorczyk A. Investigation of glycerol doping on ignition delay times and laminar burning velocities of gasoline and diesel fuel. Combust Engines 2017;169:167–75.
[14] Eaton SJ, Wallace TT, Sarnacki BG, Lokocz Adams T, Kimball RW, Henry JA, et al. Combustion and emissions of a glycerol-biodiesel emulsion fuel in a medium-speed engine. J Mar Eng Technol 2019;18:102–11.
[15] Emberson DR, Wyndorps J, Ahmed A, Bjørgen KOP, Løvås T. Detailed examination of the combustion of diesel/glycerol emulsions in a compression ignition engine. Fuel 2021;291:120147.
[16] Szori M, Giri BR, Wang Z, Dawood AE, Viskolcz B, Farooq A. Glycerol carbonate as a fuel additive for a sustainable future. Sustain Energy Fuels 2018;2:2171–8.
[17] Kraft M, Maigaard P, Mauss F, Christensen M, Johansson B. Investigation of combustion emissions in a homogeneous charge compression injection engine: Measurements and a new computational model. Proc Combust Inst 2000;28:1195–201.
[18] Tuner M, Pasternak M, Mauss F, Bensler H. A PDF-based model for full cycle simulation of direct injected engines. SAE technical paper, 2008-01-1606, 2008.
[19] Pasternak M, Mauss F, Perlman C, Lehtiniemi H. Aspects of 0D and 3D modeling of soot formation for diesel engines. Combust Sci Technol 2014;186:1517–35.
[20] Franken T, Sommerhoff A, Willvems W, Matrisciano H, Borg A, et al. Advanced predictive diesel combustion simulation using turbulence model and stochastic reactor model. SAE technical paper, 2017-01-0516, 2017.
[21] Korsunovs A, Campean F, Pant G, Garcia-Afonso O, Tunc E. Evaluation of zero-dimensional stochastic reactor modelling for a diesel engine application. Int J Engine Res 2020;21:592–609.
[22] Franken T, Matrisciano A, Sari R, Robles AF, Serrano-Monsalve J, Pintor DL, et al. Modeling of reactivity controlled compression ignition combustion using a stochastic reactor model coupled with detailed chemistryl. SAE technical paper, 2021-24-0014, 2021.
[23] Matrisciano A, Pasternak M, Wang X, Antoshkiv O, Mauss F, Berg P. On the performance of biodiesel blends-experimental data and simulations using a stochastic fuel test bench. SAE technical paper, 2014-01-1115, 2014.
[24] Yasar H, Usta E, Demir U. Experimental and stochastic reactor modeling results of an HCCI engine fueled with primary reference fuel. Energy Fuels 2018;32:2497–505.
[25] Ahmedi A, Ahmed SS, Kalghatgi GT. Simulating combustion in a PCI (premixed compression ignition) engine using DI-SRM and 3 components surrogate model. Combust Flame 2015;162:3728–39.
[26] Maurya RK, Mishra P. Parametric investigation on combustion and emissions characteristics of a dual fuel (natural gas port injection and diesel pilot injection) engine using 0-D SRM and 3D CFD approach. Fuel 2017;210:900–13.
[27] Maurya RK, Akhil N. Development of a new reduced hydrogen combustion mechanism with NOx and parametric study of hydrogen HCCI combustion using stochastic reactor model. Energy Convers Manage 2017;132:65–81.
[28] Maurya RK, Akhil N. Numerical investigation of ethanol fuelled HCCI engine using stochastic reactor model. Part 1: Development of a new reduced ethanol oxidation mechanism. Energy Convers Manage 2016;118:44–54.
[29] Srivastava DK, Agarwal AK, Gupta T. Effect of engine load on size and number distribution of particulate matter emitted from a direc injection compression ignition engine. Aerosol Air Qual Res 2011;11:915–20.
[30] Maurya RK, Saxena MR, Rai P, Bhardwaj A. Effect of compression ratio, nozzle opening pressure, engine load, and butanol addition on nanoparticle emissions from a non-road diesel engine. Environ Sci Pollut Res 2018;25:14674–89.
[31] Saxena MR, Maurya RK. Optimization of engine operating conditions and investigation of nano-particle emissions from a non-road engine fuelled. Biofuels 2020;11:543–60.

[32] Karavalakis G, Hajbabaei M, Jiang Y, Yang J, Johnson KC, Cocker DR, et al. Regulated, greenhouse gas, and particulate emissions from lean-burn and stoichiometric natural gas heavy-duty vehicles on different fuel compositions. Fuel 2016;175:146–56.
[33] Raza M, Chen L, Leach F, Ding S. A review of particulate number (PN) emissions from gasoline direct injection (GDI) engines and their control techniques. Energies 2018;11:1417.
[34] Maricq MM, Xu N. Comprehensive kinetic modeling and experimental study of a fuel-rich, premixed n-heptane flame. Aerosol Sci 2004;35:1251–74.
[35] Kim W-G, Kim C-K, Lee J-T, Yun C-W, Yook S-J. Characteristics of nanoparticle emission from a light-duty diesel vehicle during test cycles simulating urban rush-hour driving patterns. J Nanoparticle Res 2018;20:94.
[36] Veynante D, Vervisch V. Turbulent combustion modeling. Prog Energy Combust Sci 2002;28:193–266.
[37] Haworth DC. Progress in probability density function methods for turbulent reacting flows. Prog Energy Combust Sci 2010;36:168–259.
[38] Pozorski J, Wacławczyk M. Mixing in turbulent flows: An overview of physics and modelling. Processes 2020;8:1379.
[39] LOGE AB, LOGEsoft v3.0 Software Manuals. 2017.
[40] Pope SB. PDF methods for turbulent reactive flows. Prog Energy Combust Sci 1985;11:19–192.
[41] Lewandowski MT, Netzer C, Emberson D, Løvås T. Numerical investigation of optimal flow conditions in an optically accessed compression ignition engine. Transp Eng 2020;2:100036.
[42] Pasternak M, Mauss F, Lange F. Time dependent based mixing time modelling for diesel engine combustion simulations. In: Dynamics of explosions and reactive systems (ICDERS), 24–29 July. Irvine, CA. 2011.
[43] Kozuch P. Phenomenological model for a combined nitric oxide and soot emission calculation in DI diesel engines [Ph.D. thesis], Stuttgart, Germany; 2004.
[44] Stein SE, Walker JA, Suryan MM, Fahr A. A new path to benzene in flames. Symp (Int) Combust 1991;23(1):85–90.
[45] Weissman M, Benson SW. Mechanism of soot initiation in methane systems. Prog Energy Combust Sci 1989;15(4):273–85,.
[46] Mauß Fabian. Entwicklung eines kinetischen Modells der Rußbildung mit schneller Polymerisation [Ph.D. thesis], 1st ed. Cuvillier Verlag; 1998.
[47] Frenklach M, Wang H. Detailed modeling of soot particle nucleation and growth. Symp (Int) Combust 1991;23(1):1559–66, Twenty-Third Symposium (International) on Combustion.
[48] Zeuch Thomas, Moréac Gladys, Ahmed Syed Sayeed, Mauss Fabian. A comprehensive skeletal mechanism for the oxidation of n-heptane generated by chemistry-guided reduction. Combust Flame 2008;155(4):651–74,.
[49] Frenklach Michael. Method of moments with interpolative closure. Chem Eng Sci 2002;57(12):2229–39, , Population balance modelling of particulate systems.
[50] Ahmed A, Goteng G, Shankar VSB, Al-Qurashi K, Roberts WL, Sarathy SM. A computational methodology for formulating gasoline surrogate fuels with accurate physical and chemical kinetic properties. Fuel 2015;143:290–300.
[51] Seidel L, Netzer C, Hilbig M, Mauss F, Klauer C, Pasternak M, et al. Systematic reduction of detailed chemical reaction mechanisms for engine applications. ASME J Eng Gas Turbines Power 2017;139:091701.
[52] Ranzi E, Frassoldati A, Grana R, Cuoci A, Faravelli T, Kelley AP, et al. Hierarchical and comparative kinetic modeling of laminar flame speeds of hydrocarbon and oxygenated fuels. Prog Energy Combust Sci 2012;38:468–501.
[53] Barker Hemings E, Cavallotti C, Cuoci A, Faravelli T, Ranzi E. A detailed kinetic study of pyrolysis and oxidation of glycerol (propane-1,2,3-triol). Combust Sci Technol 2012;184:1164–78.
[54] Dee V, Shaw BD. Combustion of propanol–glycerol mixture droplets in reduced gravity. Int J Heat Mass Transfer 2004;47:4857–67.
[55] Wenming Y, Meng Y. Phi-T map analysis on RCCI engine fueled by methanol and biodiesel. Energy 2019;187:115958.
[56] Netzell K, Harry Lehtiniemi H, Mauss F. Calculating the soot particle size distribution function in turbulent diffusion flames using a sectional method. Proc Combust Inst 2007;31:667–74.